

Broken Power-law Distributions from Low Coronal Compression Regions or Shocks

N. A. Schwadron¹, M. A. Lee¹, M. Gorby¹, N. Lugaz¹, H. E. Spence¹, M. Desai², T. Török³, C. Downs³, J. Linker³, R. Lionello³, Z. Mikić³, P. Riley³, J. Giacalone⁴, J. R. Jokipii⁴, J. Kota⁴ and K. Kozarev⁵

¹ University of New Hampshire, Durham, NH, 03824

² Southwest Research Institute, San Antonio, TX 78228, USA

³ Predictive Science Inc., San Diego, CA 92121

⁴ University of Arizona, Tucson, AZ 85721

⁵ Harvard-Smithsonian Center for Astrophysics, Cambridge, Mass 02138

E-mail: n.schwadron@unh.edu

Abstract. Coronal Mass Ejection (CME) expansion regions low in the corona ($< 2 - 3 R_s$) are highly efficient for the acceleration of energetic particles. Because the acceleration occurs over a finite spatial region, there is a regime where particles diffuse away and escape from the acceleration sites, leading to the formation of broken power-law distributions. This paper highlights recent results indicating that CME expansion and acceleration in the low corona may cause rapid particle acceleration and create large solar energetic particle events with broken power-law distributions.

1. Introduction

The low corona creates the conditions necessary for rapid particle acceleration. Sophisticated CME simulations have shown that diffusive shock acceleration at driven shocks may be responsible for accelerating solar energetic protons up to very high energies of 10 GeV for very strong shocks [1–4].

[5] showed results of the Energetic Particle Radiation Environment Model [EPREM, 6] for describing particle acceleration in the corona. The model includes an energetic particle solver describing the evolution of the particle distribution using the focused transport equation. The particle acceleration and propagation model requires information about the evolution of the plasma based on simulated magnetohydrodynamic (MHD) fields.

The MHD fields are solved using CORHEL (Corona-Heliosphere) for the ambient solar corona, solar wind [7–9] and CMEs. CORHEL is based on the MAS (Magnetohydrodynamic Algorithm outside a Sphere) code [e.g., 10–12] that solves standard viscous and resistive MHD equations in spherical coordinates. The model incorporates an empirical coronal heating function, thermal conduction parallel to the magnetic field, and radiative losses.

Rapid particle acceleration in the low corona after fast CME expansion is often traced back to large-scale compression regions or shocks near the expanding CME legs [5; 13; 14]. In the cases of particle acceleration from compression regions [see 15; 16] and from shocks [e.g., 17; 18], particles rapidly scatter across the structure and gain energy after each crossing of



the compression gradient or shock. The total energy gain for shocks depends on the number of shock crossings [19; 20]. In the case of compressions, the situation is more complex since different scattering events sample different parts of the compression and therefore lead to varying gains in energy. Diffusive acceleration often requires a quasi-perpendicular configuration [21–23] or a short scattering mean free path [24–26] for efficient particle acceleration.

The common occurrence of broken power-law distributions [27–30] is another important observational factor in the development of our understanding large SEP events, particularly ground level events. [31] find that the power-law break has a strong rigidity dependence, suggesting strong wave-particle interactions. **The effects of shock geometry on spectral breaks has been modeled by [32] based on temporally limited particle acceleration.**

The formation of the broken power law remains an important problem. In this paper, we show how broken-power law distributions can result from size-limited shocks or compressions that often form in the low corona. **We note that the basic elements of this physical process have parallel analogs in Earth’s magnetotail. Though in a different part of parameter space (subsonic flow versus shocks) charged particles are energized in the magnetotail through adiabatic compression and through energy-dependent gradient drifts along electric fields, which are controlled fundamentally by the finite dimensions of the system. These factors in turn produce non-Maxwellian particle distributions with spectral breaks [33–35], demonstrating the ubiquity of these same governing processes that are the focus of this work for which the complexity is much greater.**

2. Diffusive Particle Acceleration at Low Coronal Shocks and Compressions

Our analysis is motivated, in part, by recent results of CME simulations, which reveal how a CME rapidly accelerated low in the corona causes extremely strong compression regions [5]. Consider the configuration in Figure 1. A compression or shock region is driven by a CME expansion and acceleration. Notably the compression is strongest where the CME acceleration or expansion is most rapid [36].

Diffusive acceleration at shocks is solved for using the Parker transport equation:

$$\frac{\partial f}{\partial t} + \mathbf{u} \cdot \nabla f - \nabla \cdot (\mathbf{K} \cdot \nabla f) - \frac{\nabla \cdot \mathbf{u}}{3} p \frac{\partial f}{\partial p} = Q_0 \delta(x) \delta(z) \delta(p - p_{inj}) \quad (1)$$

where

$$\mathbf{K} = \kappa_{\parallel} \hat{e}_b \hat{e}_b + \kappa_{\perp} (\mathbf{I} - \hat{e}_b \hat{e}_b) \quad (2)$$

and κ_{\parallel} and κ_{\perp} are coefficients of diffusion parallel and perpendicular to the magnetic field, respectively. The distribution function is given by f , the plasma velocity is given by \mathbf{u} , and the **particle momentum in the plasma frame is given by p** . The diffusion tensor indicated here is diagonal and neglects an off-diagonal term, κ_A , due to drift is sometimes included in the diffusion tensor.

The source term represents a modification of the standard approach to diffusive shock acceleration theory. In the standard treatment, particles are injected at a fixed energy, the injection energy, and at the location of the shock ($x = 0$). The shock or compression is within the y - z plane centered on $x = 0$. Magnetic field lines lie within plane of coplanarity x - z . **Particles injected at a fixed location $z = 0$ are accelerated while the field connection point sweeps across the shock structure.** A similar concept was used to model particle acceleration at the blunt termination shock [37].

To develop a quantitative description, we solve for a Green’s function for injection at a fixed location, at $z = 0$. We then integrate over the region along the shock, from $z = 0$ to $z = L$. The

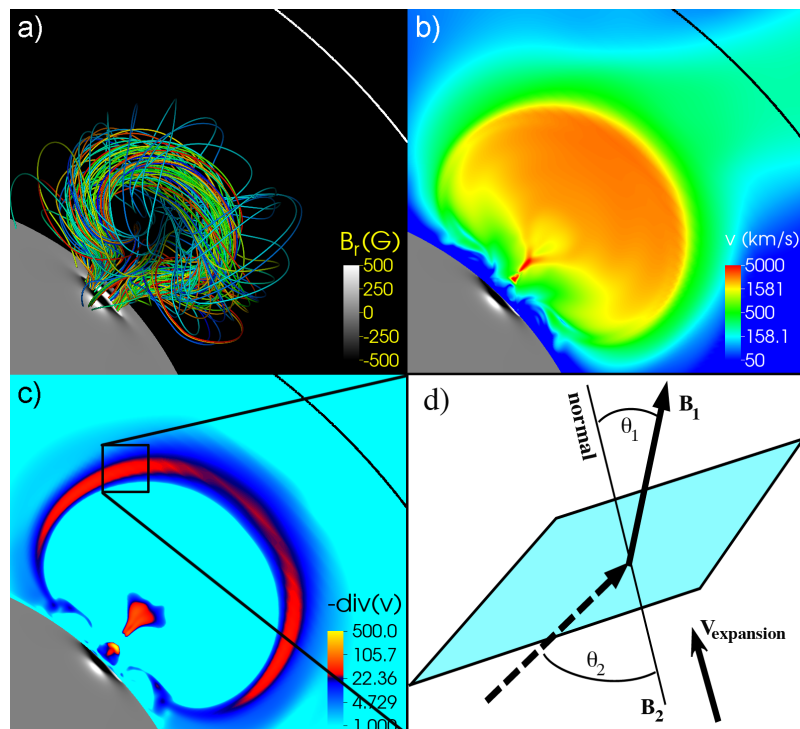


Figure 1. (From [36]). Strong compression from the expansion of a CME in the low corona leads to rapid particle acceleration [5]. The erupting magnetic flux rope (Panel a) is shown along with the photospheric field strength B_r (greyscale on the solar surface). The CME accelerates rapidly (Panel b). Strong compressions or shocks are formed, **showing strong velocity divergence, $\nabla \cdot \mathbf{u}$ (Panel c) expressed in code units corresponding to $7 \times 10^{-4} \text{ s}^{-1}$** . The blow out (Panel d) shows a magnetic flux bundle piercing the shock.

source-term scaling constant Q_0 is

$$Q_0 = u_1 \epsilon f_{\text{inj}} L p_{\text{inj}} \quad (3)$$

where u_1 is the upstream flow speed in the frame of the shock and the injection efficiency is given by ϵ . The distribution function at the injection energy is f_{inj} , and the size-scale of the shock is given by L .

We track $\nabla \cdot \mathbf{V}$ in Figure 2 along a magnetic flux bundle. The acceleration region is most pronounced where the CME expansion and acceleration is strongest. The outward CME expansion speed is $< 600 \text{ km/s}$ at 1.5 solar radii. By the time this expansion reaches 1.8 solar radii, the speed reaches $\sim 1500 \text{ km/s}$. Above 1.8 solar radii the acceleration of the CME slows and the speed levels off at $\sim 1400 \text{ km/s}$. The divergence shown in Figure 2 (right panels) provides an excellent indicator for the pronounced effects of the CME expansion and acceleration. This divergence is largest between 1.5 and 2 solar radii and then levels off at larger distances.

The Parker transport equation (1) includes the divergence in the plasma velocity (4th term on left-hand-side). This term leads to the acceleration of energetic particles. The CME acceleration is prompt and localized (between 1.5 and 2 solar radii) leading to prompt energetic particle acceleration inside of 2 solar radii.

The configuration of the accelerator provides a connection point between the shock or compression and a magnetic field line (or flux bundle) that moves along the structure. This motion occurs as particles are accelerated. On average, the higher the energy that particles gain,

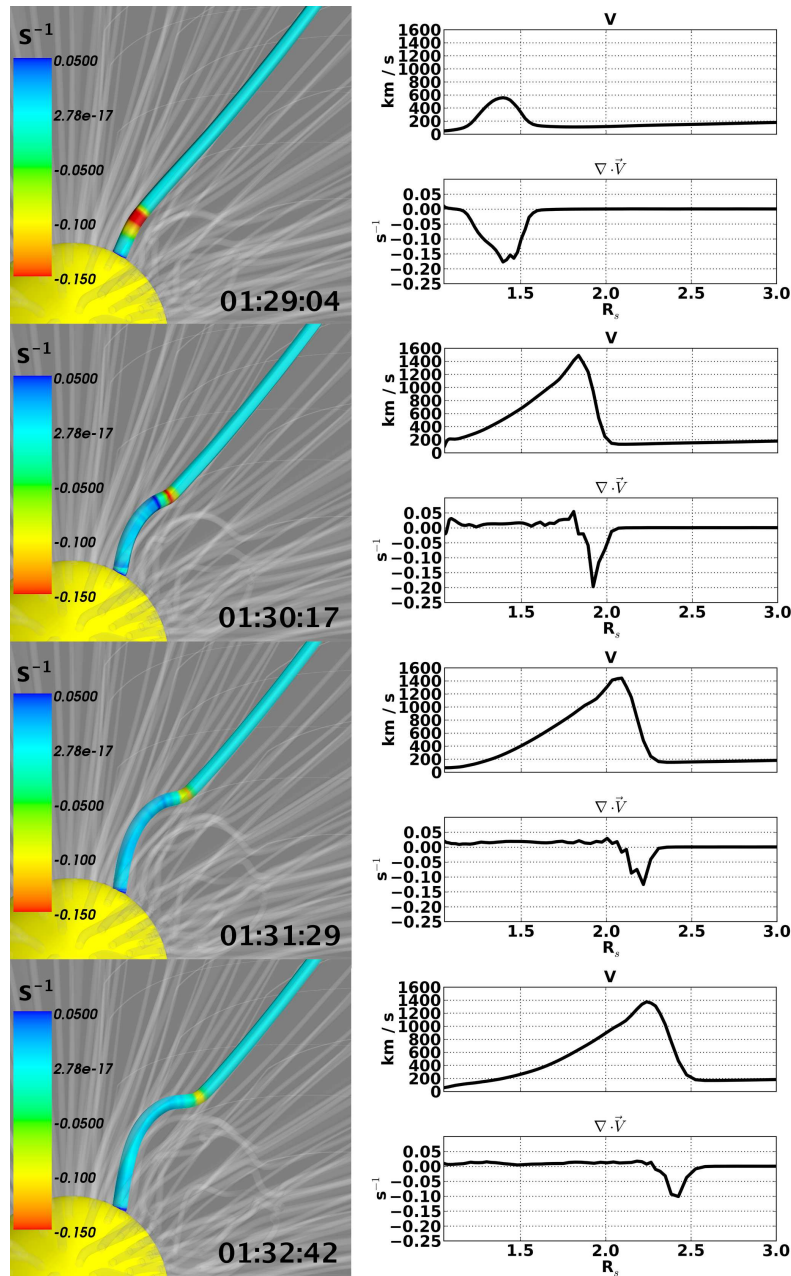


Figure 2. [From 36] The development of a compression region viewed on a bundle of field lines. Right: the curves show V and $\nabla \cdot \mathbf{V}$ along the field line bundle during CME expansion at four different instances within the simulation. Left: Configuration of the magnetic flux bundle (depicted as a tube) deformed by the CME expansion. Color-coding indicates $\nabla \cdot \mathbf{V}$. Indicated times are hh:mm:ss, where time zero corresponds to the release of the CME.

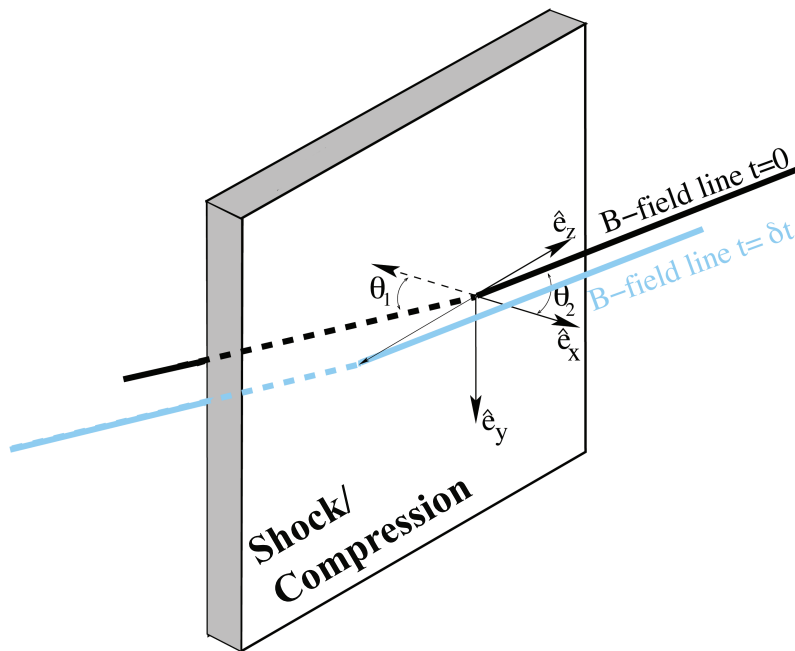


Figure 3. [From 36] Diagram of a magnetic flux bundle piercing a shock or compression region as a function of time. The initial flux bundle ($t = 0$ in black) convects through the shock or compression as the field-line footprint (flux bundle at $t = \delta t$ in blue) moves across the structure.

the longer the flux bundle where these particles are accelerated has remained in contact with the shock or compression. A flux bundle connection point eventually moves off of the accelerator, which limits the particles' energy gain and leads to the formation of a broken power-law or exponential roll-over in the particle distribution.

We use the following expressions for the diffusion coefficient

$$\mathbf{K} = \kappa_{\parallel} \hat{e}_b \hat{e}_b + \kappa_{\perp} (\mathbf{I} - \hat{e}_b \hat{e}_b) \quad (4)$$

where the diffusion coefficient component projections are

$$\kappa_{xx} = \kappa_{\parallel} \cos^2 \theta + \kappa_{\perp} \sin^2 \theta \quad (5)$$

$$\kappa_{xz} = (\kappa_{\parallel} - \kappa_{\perp}) \sin \theta \cos \theta \quad (6)$$

$$\kappa_{zz} = \kappa_{\parallel} \sin^2 \theta + \kappa_{\perp} \cos^2 \theta \quad (7)$$

Consider steady state injection of particles at $z = 0$ and $x = 0$ with momentum p_{inj} :

$$\mathbf{u} \cdot \nabla f - \nabla \cdot (\mathbf{K} \cdot \nabla f) - \frac{\nabla \cdot \mathbf{u}}{3} p \frac{\partial f}{\partial p} = Q_0 \delta(x) \delta(z) \delta(p - p_{inj}) \quad (8)$$

We take (x, z) as the coplanarity plane and no dependence on y , so that cross-field drifts do not appear (see Figure 3). The scattering mean free path is $\lambda_{\parallel} = \lambda_{\parallel 0} (R_g/R_{g0})^x$ where $R_g = pc/q$ is the particle rigidity and $R_{g0} = (m_p v_0 c/e)(A_0/Z_0)$ is a reference rigidity at mass $m_0 = A_0 m_p$, charge $q_0 = Z_0 e$ and speed v_0 . We adopt a 1 AU mean free path of 0.14 AU and use a $1/B$ scaling into the low corona, which is typical for observationally constrained values [38]. Taking a 1 G field in the corona, we find a reference scattering mean free path of $\lambda_{\parallel 0} = 0.015 R_s$ at $T_0 = 1$ MeV/nuc.

We now explicitly expand the differential equation,

$$\begin{aligned} u_x \frac{\partial f}{\partial x} + u_z \frac{\partial f}{\partial z} - \nabla \cdot (\kappa_{\perp} \mathbf{l} \cdot \nabla f) - \nabla \cdot [\hat{e}_b (\kappa_{\parallel} - \kappa_{\perp}) \hat{e}_b \cdot \nabla f] \\ + \frac{u_{x1} - u_{x2}}{3} \delta(x) p \frac{\partial f}{\partial p} = Q_0 \delta(x) \delta(z) \delta(p - p_{inj}). \end{aligned} \quad (9)$$

and perform the Fourier transform,

$$f(z, x, p) = \frac{1}{2\pi} \int_{-\infty}^{\infty} dk \exp(ikz) \tilde{f}(k, x, p), \quad (10)$$

such that

$$\begin{aligned} u_x \frac{\partial \tilde{f}}{\partial x} + ik u_z \tilde{f} + k^2 \kappa_{zz} \tilde{f} - \frac{\partial}{\partial x} \left(\kappa_{xx} \frac{\partial \tilde{f}}{\partial x} \right) - \frac{\partial}{\partial x} [\kappa_{xz} ik \tilde{f}] \\ - ik \kappa_{xz} \frac{\partial \tilde{f}}{\partial x} + \delta(x) \frac{u_{1x} - u_{2x}}{3} \frac{\partial \tilde{f}}{\partial \ln p} = Q_0 \delta(x) \delta(p - p_{inj}). \end{aligned} \quad (11)$$

We take $\tilde{f} \propto \exp(\alpha x)$ for $x \neq 0$ which requires the following condition when taking into account upstream and downstream conditions:

$$-\alpha^2 \kappa_{xx} + \alpha(u_x - 2ik\kappa_{xz}) + ik u_z + k^2 \kappa_{zz} = 0 \quad (12)$$

The upstream solution, $j = 1$, and downstream solution, $j = 2$, are

$$\alpha_j = \frac{u_{xj}}{2\kappa_{xxj}} - ik \frac{\kappa_{xzj}}{\kappa_{xxj}} + \frac{(-1)^{j+1}}{\kappa_{xxj}} \sqrt{u_{xj}^2/4 + \kappa_{\parallel j} \kappa_{\perp j} k^2 + ik(\kappa_{xxj} u_{zj} - \kappa_{xzj} u_{xj})}. \quad (13)$$

Conventionally, the signs, $(-1)^{j+1}$, are chosen for convergence so that for $k = 0$, we recover the result for a stationary shock.

Given α_j , we integrate equation (11) from the upstream to downstream side of the shock or compression. This integral extends over a narrow region centered on the shock jump. We recover the following equation:

$$-(\kappa_{xx2} \alpha_2 - \kappa_{xx1} \alpha_1) \tilde{f} - (\kappa_{xz2} - \kappa_{xz1}) ik \tilde{f} + \frac{\Delta u}{3} \frac{\partial \tilde{f}}{\partial \ln p} = Q_0 \delta(p - p_{inj}) \quad (14)$$

We find the property

$$\begin{aligned} (\kappa_{xx2} \alpha_2 - \kappa_{xx1} \alpha_1) + (\kappa_{xz2} - \kappa_{xz1}) ik = \\ -\frac{\Delta u}{2} - \sum_{j=1}^2 \sqrt{\frac{u_{xj}^2}{4} + \kappa_{\parallel j} \kappa_{\perp j} k^2 + ik(\kappa_{xxj} u_{zj} - \kappa_{xzj} u_{xj})} \end{aligned} \quad (15)$$

We now express the solution for $\tilde{f}(k, p)$, and the distribution function at the shock or compression:

$$\begin{aligned} f_s(z, p) = \frac{3Q_0}{2\pi \Delta u p_{inj}} \left(\frac{p}{p_{inj}} \right)^{-3/2} \int_{-\infty}^{\infty} dk \\ \times \exp \left(ikz - \frac{3}{\Delta u} \int_{\ln p_{inj}}^{\ln p} d \ln p' \sum_{j=1}^2 \sqrt{\frac{u_{xj}^2}{4} + \kappa_{\parallel j} \kappa_{\perp j} k^2 + ik(\kappa_{xxj} u_{zj} - \kappa_{xzj} u_{xj})} \right). \end{aligned} \quad (16)$$

Here $\Delta u = u_{1x} - u_{2x}$.

Note that the square root in equation (16) equals $u_{xj}/2$ as $k \rightarrow 0$. We add and subtract $u_{xj}/2$ from the square root; the $\ln p$ -integral of $u_{xj}/2$ is trivial and we obtain

$$f_s(z, p) = \frac{3Q_0}{2\pi\Delta u p_{inj}} \left(\frac{p}{p_{inj}} \right)^{-\gamma} \int_{-\infty}^{\infty} dk \exp(ikz) \times \exp \left(-\frac{3}{\Delta u} \int_{\ln p_{inj}}^{\ln p} d \ln p' \sum_{j=1}^2 \left[\sqrt{\frac{u_{xj}^2}{4} + \kappa_{\parallel j} \kappa_{\perp j} k^2 + ik(\kappa_{xxj} u_{zj} - \kappa_{xzzj} u_{xj})} - \frac{u_{xj}}{2} \right] \right) \quad (17)$$

where $\gamma = 3r_c/(r_c - 1)$ is the power law index of diffusive shock acceleration. Assuming that the protons are non-relativistic ($p \approx mv$), and noting that the square root is a function of $k(v')^{\chi+1}$, we rewrite (17) as

$$f_s(z, p) = \frac{3Q_0}{2\pi\Delta u p_{inj}} \left(\frac{v}{v_{inj}} \right)^{-\gamma} \frac{1}{v^{\chi+1}} \int_{-\infty}^{\infty} d\eta \exp \left[i\eta(z/v^{\chi+1}) - \frac{3}{(\chi+1)\Delta u} \times \int_{-\infty}^{\ln(\eta)} d \ln \xi \sum_{j=1}^2 \left\{ \sqrt{\frac{u_{xj}^2}{4} + \frac{\tau_{\parallel j} \tau_{\perp j}}{9} \xi^2 + i\xi \left(\frac{\kappa_{xxj}}{v^{\chi+1}} u_{zj} - \frac{\kappa_{xzzj}}{v^{\chi+1}} u_{xj} \right) - \frac{u_{xj}}{2}} \right\} \right] \quad (18)$$

where $\xi = k(v')^{\chi+1}$, $\eta = kv^{\chi+1}$, $\kappa_{\parallel} = \tau_{\parallel} v^{\chi+1}/3$, $\kappa_{\perp} = \tau_{\perp} v^{\chi+1}/3$, and the lower limit of the ξ -integration is replaced by $-\infty$ since the integrand is convergent as $kv_{inj}^{\chi+1} \rightarrow 0$. **We have assumed here that $\kappa_{\perp}/\kappa_{\parallel} = \text{constant}$. However, non-linear guiding center (NLGC) theory predicts that κ_{\perp} and κ_{\parallel} have different dependence on particle speed [39; 40]. Future studies will need to investigate the effects of these alternative behaviors for the differential energy spectrum, and behavior of heavy ions.**

The η -integral purely a function of $z/v^{\chi+1}$. If $v^{\chi+1}/z > \eta_0$, where η_0 is the scale for the integration decay, then the factor $\exp[i\eta(z/v^{\chi+1})] \approx 1$ and (18) yields the high-energy power-law spectrum, $f_s \propto v^{-\gamma-1-\chi}$. For small and intermediate values of $v^{\chi+1}/z$ ($v^{\chi+1}/z \ll \eta_0$ and $v^{\chi+1}/z \sim \eta_0$) we expand the integrand in powers of ξ and retain terms up to order ξ^2 . The ξ -integral is evaluated,

$$f_s(z, p) = \frac{3Q_0}{2\pi\Delta u p_{inj}} \left(\frac{v}{v_{inj}} \right)^{-\gamma} \frac{1}{v^{\chi+1}} \times \int_{-\infty}^{\infty} d\eta \exp \left[i\eta \frac{z}{v^{\chi+1}} - \frac{3}{(\chi+1)\Delta u} (i\eta a + \eta^2 b/4) \right] \quad (19)$$

where

$$a = \sum_{j=1}^2 \left[\frac{\kappa_{xxj} u_{zj}}{v^{\chi+1} u_{xj}} - \frac{\kappa_{xzzj}}{v^{\chi+1}} \right] \quad (20)$$

$$b = \sum_{j=1}^2 \left\{ 2 \frac{\tau_{\parallel j} \tau_{\perp j}}{9 u_{xj}} + \frac{2}{u_{xj}} \left[\frac{\kappa_{xxj} u_{zj}}{v^{\chi+1} u_{xj}} - \frac{\kappa_{xzzj}}{v^{\chi+1}} \right]^2 \right\} \quad (21)$$

The remaining integration in (19) is evaluated by “completing the square”. We obtain

$$f_s(z, p) \approx \frac{3Q_0}{2\pi\Delta u p_{inj}} \left(\frac{v}{v_{inj}} \right)^{-\gamma} \frac{1}{v^{\chi+1}} \sqrt{\frac{8\pi\Delta u}{3b}} \times \exp \left\{ - \left[\frac{z}{v^{\chi+1}} - \frac{3a}{(\chi+1)\Delta u} \right]^2 \left(\frac{(\chi+1)\Delta u}{3b} \right) \right\} \quad (22)$$

Since it takes time for ions to be accelerated to high energies, the peak of the ion distribution moves from the point of injection to progressively more distant regions on the shock or compression flank. The quantity

$$z_d = \frac{3av^{\chi+1}}{(\chi+1)\Delta u} \quad (23)$$

is the distance moved along the shock by the majority of ions in the process of being accelerated to a given energy. The average ion speed along the shock is

$$V_{sz} = \frac{dz_d}{d\tau_p} \quad (24)$$

and τ_p is the characteristic time to accelerate ions to momentum p . The quantity $d\tau_p$ is the infinitesimal time to accelerate ions from p to $p + dp$:

$$d\tau_p = \frac{3\delta x}{\Delta u} \frac{dp}{p}. \quad (25)$$

The characteristic width of the acceleration region is

$$\delta x = \frac{\kappa_{xx1}}{u_{x1}} + \frac{\kappa_{xx2}}{u_{x2}}. \quad (26)$$

Using (24) and (25), we then solve for the average particle speed along the shock

$$V_{sz} = \frac{v^{\chi+1}a}{\delta x} \quad (27)$$

The solution for f_s is written in the form,

$$f_s(z, p) \approx \frac{3Q_0}{2\pi\Delta up_{inj}} \left(\frac{v}{v_{inj}} \right)^{-\gamma} \sqrt{\frac{\pi}{D_z}} \exp \left\{ -\frac{(z - z_d)^2}{4D_z} \right\} \quad (28)$$

where the width of the Gaussian is

$$D_z = \frac{3bv^{2(\chi+1)}}{4(\chi+1)\Delta u}. \quad (29)$$

The diffusion rate is

$$K_{szz} = \frac{dD_z}{d\tau_p} = \frac{bv^{2(\chi+1)}}{2\delta x}. \quad (30)$$

Equation 28 is used as a Green's function. We integrate injection from $z' = 0$ to L . The resulting total distribution, $F_s(z, p)$, is

$$\begin{aligned} F_s(z, p) &= \frac{1}{L} \int_0^L dz_{inj} f'_s(z, z_{inj}, p) \\ &= \frac{3Q_0}{2\Delta up_{inj}L} \left(\frac{p}{p_{inj}} \right)^{-\gamma} \left[\operatorname{erf} \left(\frac{L + z_d - z}{2\sqrt{D_z}} \right) - \operatorname{erf} \left(\frac{z_d - z}{2\sqrt{D_z}} \right) \right]. \end{aligned} \quad (31)$$

Figure 4 shows the spectrum in the case in which there is no escape of particles from the shock accelerator. In this case we have considered an obliquity angle of $\theta = 70^\circ$ at 2 solar radii,

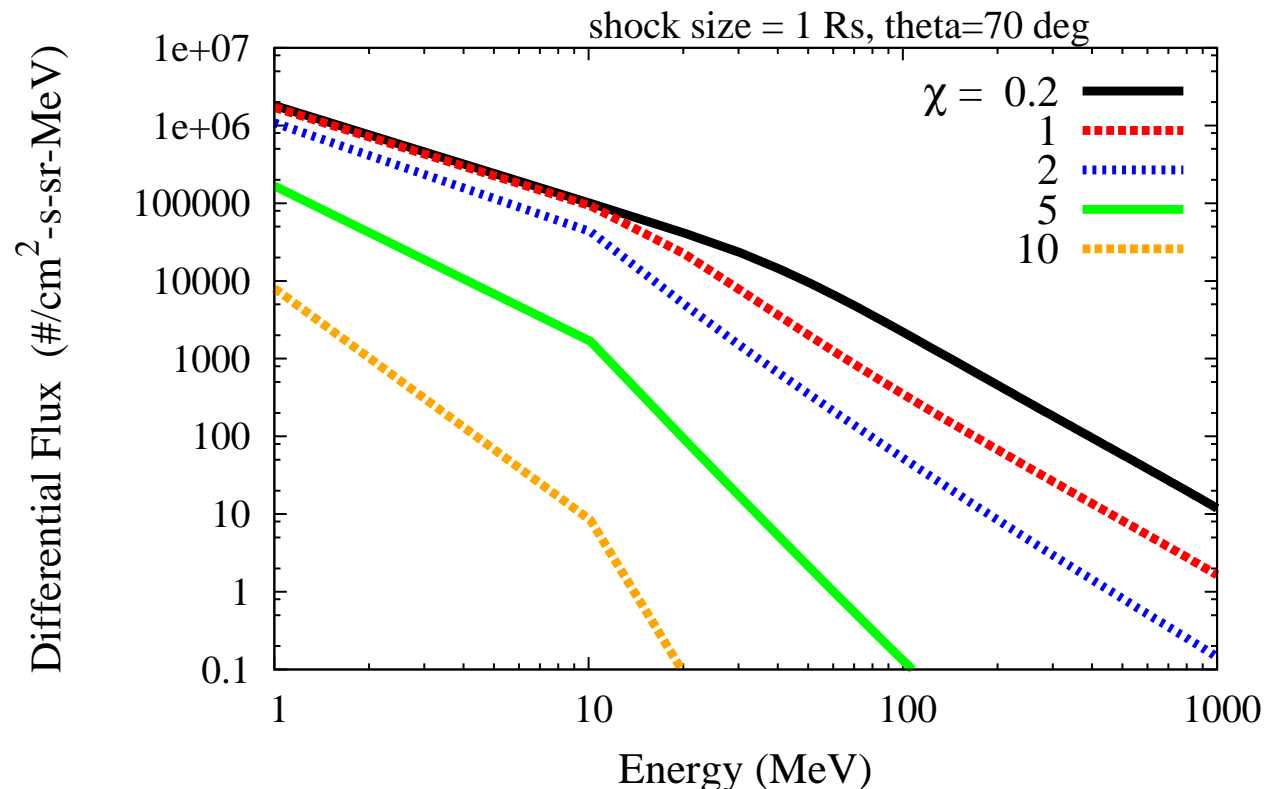


Figure 4. Differential spectra for several cases of χ based on equation 31. Note the spectral break and the relatively smooth power-law at higher energies. The spectral break drops with energy for increasing values of χ . These spectra are formed at $r \sim 2 R_s$, a shock or size of $1 R_s$ and an obliquity angle of $\theta = 70^\circ$.

with a shock size of $1 R_s$. We have also taken a compression ratio of 3. By comparison, Figure 5 shows a similar case with a smaller shock size of $0.25 R_s$ and Figure 6 shows a shock size of $1 R_s$ but an obliquity angle of $\theta = 30^\circ$. In each of these cases, we have taken a ratio of perpendicular to parallel diffusion of $\kappa_\perp/\kappa_\parallel = 0.01$.

Taken together Figures 4, 5 and 6 show a number of important features. First, the variation with χ shows that stronger rigidity in the scattering mean free path leads to sharper breaks in the broken power-law distribution. It is likely that stronger rigidity dependence arises through more significant wave-particle interactions, which tend to occur when the shocks or compressions are closer to being quasi-parallel.

When we compare Figure 4 and Figure 5, it is evident that the larger shock size leads to higher energies for the spectral break. This increase in the break energy seen in Figure 4 is most pronounced in instances when the the rigidity dependence is weak. This suggests that weak rigidity dependence, likely associated with quasi-perpendicular shocks, would likely result in higher energies of the spectral break, particularly for large shocks or compressions.

When we compare Figure 4 and Figure 6, we observe that the break in the power-law drops in energy for decreased obliquity angles. As in the previous case, this decrease in the break energy is most pronounced for a weak rigidity dependence in the scattering mean free path. This shows that, regardless of the rigidity dependence, a quasi-parallel shock tends to generate lower energy spectral breaks.

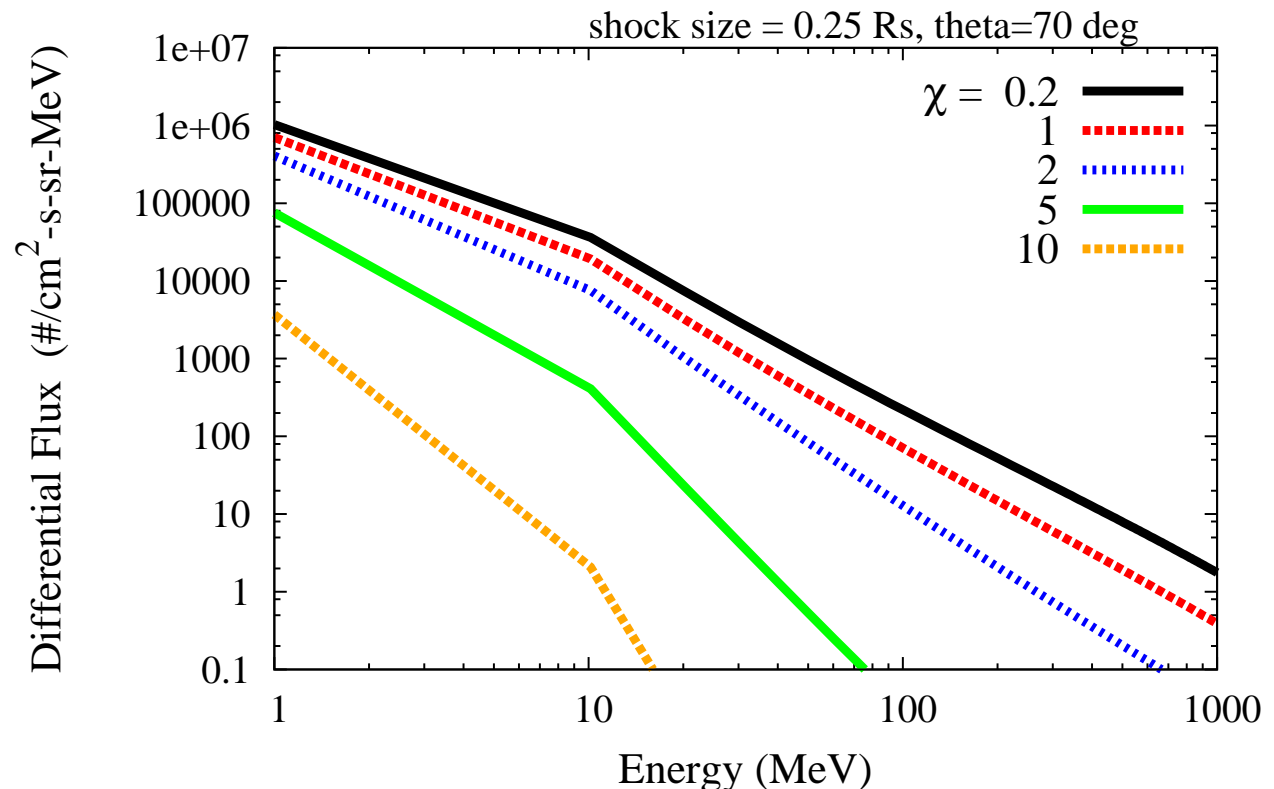


Figure 5. Differential spectra for several cases of χ based on equation 31. The conditions are the same as used in Figure 4, but the shock size is smaller, $0.25 R_s$.

3. Conclusions

Recent MHD simulations of CME expansion show the formation of strong compression regions and shocks at low coronal heights, $< 2 R_\odot$. These compressions and shocks form due to the rapid expansion and acceleration of the CME and then subside higher in the corona where the CME acceleration slows.

We developed a model of particle acceleration at a low coronal shock or compression with a finite size (length L) and a fixed field-flow angle. Results of the model show the pronounced effects of particle diffusion and particle escape, leading to double power-law distributions. The slope of the power-law below the spectral break is roughly consistent with steady diffusive shock acceleration. However, above the spectral break, the spectral slope is strongly controlled the rigidity dependence in the diffusion coefficients.

Thus, we find that strong compressions and shocks in the low corona may naturally give rise to broken power-law distributions that arise in large SEP events.

3.1. Acknowledgments

We thank all those who made C-SWEPA (NASA grant NNX13AI75G), EMMREM (grant NNX07AC14G), Sun-2-Ice (NSF grant AGS1135432), DREAM (NASA grant NNX10AB17A), and DREAM2 (NASA grant NNX14AG13A) projects possible. Data for all figures can be obtained by contacting the lead author, N. Schwadron. The contributions of T.T., C.D., R.L., J.A.L., V.A.T., Z.M., and P.R. were supported by the NSF Frontiers in Earth System Dynamics program and the Center for Integrated Space Weather Modeling, and by NASA's SBIR, HTP, LWS, and SR&T programs. Computational resources were provided by the NSF supported Texas

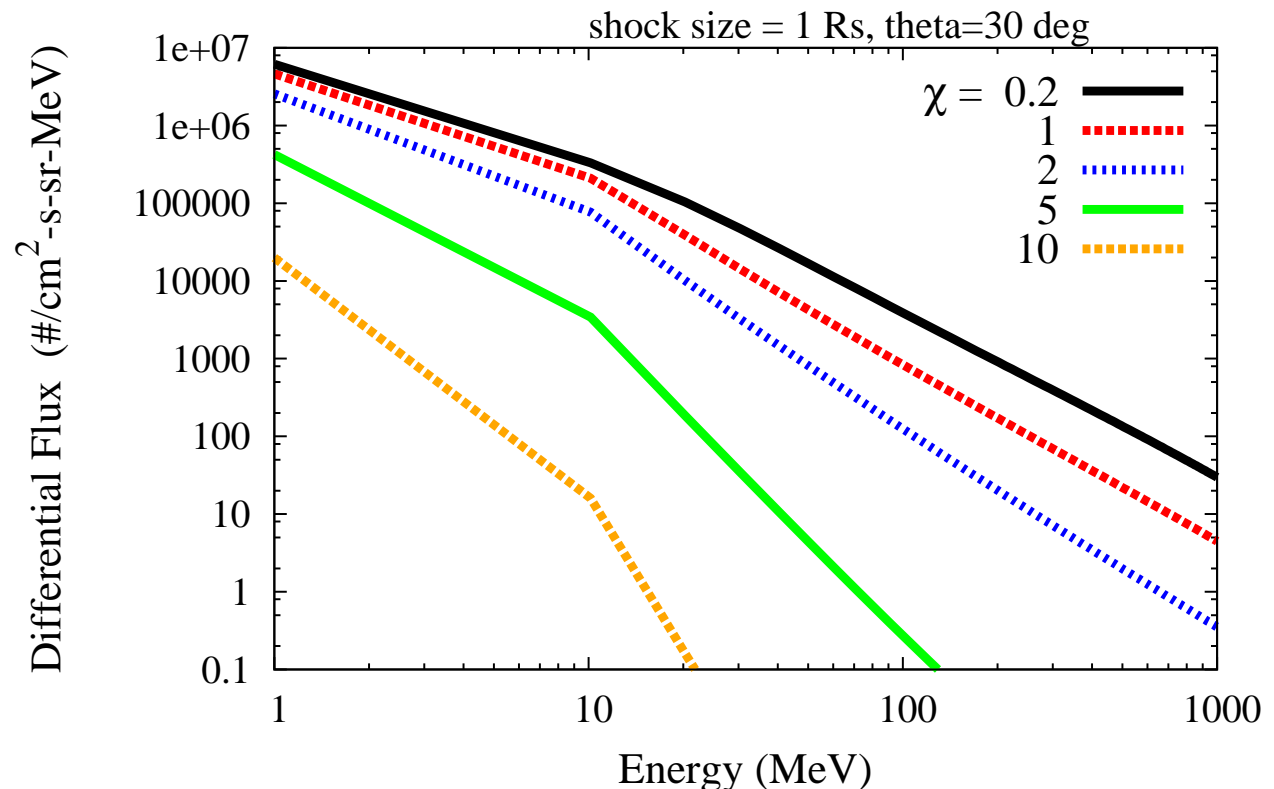


Figure 6. Differential spectra for several cases of χ based on equation 31. The conditions are the same as used in Figure 4, but the obliquity angle is $\theta = 30^\circ$.

Advanced Computing Center (TACC) in Austin and the NASA Advanced Supercomputing Division (NAS) at Ames Research Center.

References

- [1] Roussev I I, Sokolov I V, Forbes T G, Gombosi T I, Lee M A and Sakai J I 2004 *Astrophys. J. Lett.* **605** L73–L76
- [2] Manchester IV W B, Gombosi T I, De Zeeuw D L, Sokolov I V, Roussev I I, Powell K G, Kóta J, Tóth G and Zurbuchen T H 2005 *Astrophys. J.* **622** 1225–1239
- [3] Kocharov L, Lytova M, Vainio R, Laitinen T and Torsti J 2005 *Astrophys. J.* **620** 1052–1068
- [4] Tsurutani B, Wu S T, Zhang T X and Dryer M 2003 *Astron. Astrophys.* **412** 293–304
- [5] Schwadron N A, Gorby M, Török T, Downs C, Linker J, Lionello R, Mikić Z, Riley P, Giacalone J, Chandran B, Germaschewski K, Isenberg P A, Lee M A, Lugaz N, Smith S, Spence H E, Desai M, Kasper J, Kozarev K, Korreck K, Stevens M, Cooper J and MacNeice P 2014 *Space Weather* **12** 323–328
- [6] Schwadron N A, Townsend L, Kozarev K, Dayeh M A, Cucinotta F, Desai M, Golightly M, Hassler D, Hatcher R, Kim M, Posner A, PourArsalan M, Spence H E and Squier R K 2010 *Space Weather* **8** 0–+
- [7] Lionello R, Linker J A and Mikić Z 2009 *Astrophys. J.* **690** 902–912
- [8] Riley P and Lionello R 2011 *Solar Phys.* **270** 575–592
- [9] Riley P, Linker J A, Lionello R and Mikić Z 2012 *Journal of Atmospheric and Solar-Terrestrial Physics* **83** 1–10

- [10] Mikić Z and Linker J A 1994 *Astrophys. J.* **430** 898–912
- [11] Mikić Z, Linker J A, Schnack D D, Lionello R and Tarditi A 1999 *Physics of Plasmas* **6** 2217–2224
- [12] Lionello R, Mikić Z and Linker J A 1999 *Journal of Computational Physics* **152** 346–358
- [13] Gorby M J, Schwadron N A, Linker J A, Spence H E, Townsend L W and Cucinotta F A 2012 *AGU Fall Meeting Abstracts* A2216
- [14] Linker J, Mikić Z, Schwadron N, Riley P, Gorby M, Lionello R, Downs C and Torok T 2014 *40th COSPAR Scientific Assembly (COSPAR Meeting vol 40)* p 1840
- [15] Giacalone J, Jokipii J R and Kóta J 2002 *Astrophys. J.* **573** 845–850
- [16] Jokipii J R, Giacalone J and Kota J 2003 *International Cosmic Ray Conference (International Cosmic Ray Conference vol 6)* p 3685
- [17] Fermi E 1949 *Physical Review* **75** 1169–1174
- [18] Drury L O 1983 *Reports on Progress in Physics* **46** 973–1027
- [19] Bell A R 1978 *Mon. Not. R. Astr. Soc.* **182** 147–156
- [20] Bell A R 1978 *Mon. Not. R. Astr. Soc.* **182** 443–455
- [21] Jokipii J R 1982 *Astrophys. J.* **255** 716–720
- [22] Jokipii J R 1986 *J. Geophys. Res.* **91** 2929–2932
- [23] Jokipii J R 1987 *Astrophys. J.* **313** 842–846
- [24] Lee M A, Fisk L A and Skadron G 1981 *Geophys. Res. Lett.* **8** 401–404
- [25] Lee M A 1983 *J. Geophys. Res.* **88** 6109–6119
- [26] Lee M A 2005 *Astrophys. J. Suppl.* **158** 38–67
- [27] Mason G M, Wiedenbeck M E, Miller J A, Mazur J E, Christian E R, Cohen C M S, Cummings A C, Dwyer J R, Gold R E, Krimigis S M, Leske R A, Mewaldt R A, Slocum P L, Stone E C and von Rosenvinge T T 2002 *Astrophys. J.* **574** 1039–1058
- [28] Mewaldt R A, Cohen C M S, Labrador A W, Leske R A, Mason G M, Desai M I, Looper M D, Mazur J E, Selesnick R S and Haggerty D K 2005 *Journal of Geophysical Research (Space Physics)* **110** A09S18
- [29] Mewaldt R A, Cohen C M S, Mason G M, Labrador A W, Looper M L, Haggerty D E, MacLennan C G, Cummings A C, Desai M I, Leske R A, Li G, Mazur J E, Stone E C and Wiedenbeck M E 2005 *The Physics of Collisionless Shocks: 4th Annual IGPP International Astrophysics Conference (American Institute of Physics Conference Series vol 781)* ed Li G, Zank G P and Russell C T pp 227–232
- [30] Mewaldt R A, Looper M D, Cohen C M S, Haggerty D K, Labrador A W, Leske R A, Mason G M, Mazur J E and von Rosenvinge T T 2012 *Space Sci. Rev.* **171** 97–120
- [31] Desai M I, Dayeh M A, Ebert R W, McComas D J, Mason G M, Lo G, Cohen C M S, Mewaldt R A and Schwadron N A 2015 *Astrophys. J.* **To be submitted**
- [32] Li G, Zank G P, Verkhoglyadova O, Mewaldt R A, Cohen C M S, Mason G M and Desai M I 2009 *Astrophys. J.* **702** 998–1004
- [33] Kivelson M G and Spence H E 1988 *GRL* **15** 1541–1544
- [34] Spence H E and Kivelson M G 1990 *Geophys. Res. Lett.* **17** 591–594
- [35] Spence H E and Kivelson M G 1993 *J. Geophys. Res.* **98** 15487
- [36] Schwadron N A, Lee M A, Gorby M, Lugaz N, Spence H E, Desai M, Kozarev K, Török T, Downs C, Linker J, Lionello R, Mikić Z, Riley P, Giacalone J, Jokipii J R and Kota J 2015 *Astrophys. J.* **submitted**

- [37] Schwadron N A, Lee M A and McComas D J 2008 *Astrophys. J.* **675** 1584–1600
- [38] Dröge W 2005 *Advances in Space Research* **35** 532–542
- [39] Zank G P, Li G, Florinski V, Matthaeus W H, Webb G M and Le Roux J A 2004 *Journal of Geophysical Research (Space Physics)* **109** A04107
- [40] Zank G P, Li G and Verkhoglyadova O 2008 *American Institute of Physics Conference Series (American Institute of Physics Conference Series vol 1039)* ed G Li, Q Hu, O Verkhoglyadova, G P Zank, R P Lin, & J Luhmann pp 203–213